Advances in Environmental Technology 12(3) 2026, 291-307.

Iranian Reasearch Organization for Science and Technology (IROST)

Advances in Environmental Technology

Journal home page: https://aet.irost.ir

Highly efficient sunlight-powered photocatalytic degradation of rhodamine B using Cu_2Cr-LDH/TiO_2 and Cu_2Cr-LDH/BiOCl semiconductor nanocomposites

Ali Bouteiba[a,b]*, Naceur Benhadria[c,d], Nourredine Bettahar[a]

[a] *Laboratory of Inorganic Materials Chemistry and Applications (LCMIA), Faculty of Chemistry, University of Science and Technology of Oran (USTO M. B), Oran, Algeria.*

[b] *GP1/Z Complex, Liquefaction and Separation Division (LQS), Sonatrach, Béthioua, Oran, Algeria.*

[c] *Higher School of Applied Sciences of Tlemcen (ESSA-Tlemcen), Tlemcen, Algeria.*

[d] *Laboratory of Materials Chemistry (LCM), University of Oran 1 Ahmed Ben Bella, Oran, Algeria.*

ARTICLE INFO

Document Type:
Research Paper

Article history:
Received 09 September 2025
Received in revised form
23 April 2026
Accepted 02 May 2026

Keywords:
Photocatalysis
Cu_2Cr-LDH
RhB Degradation
Heterojunction formation
Sunlight-driven catalysis

ABSTRACT

This study explores the photocatalytic degradation of Rhodamine B (RhB) under sunlight irradiation using Cu_2Cr-LDH/BiOCl and Cu_2Cr-LDH/TiO_2 nanocomposites. The structural, optical, and morphological properties of the materials were thoroughly examined by X-ray diffraction (XRD), Ultraviolet–visible spectroscopy (UV-vis), X-ray photoelectron spectroscopy (XPS), and scanning electron microscopy (SEM). The primary objective was to assess the photocatalytic efficiency of these nanocomposites in degrading RhB dye under sunlight. The Cu_2Cr-LDH/BiOCl nanocomposite exhibited superior photocatalytic performance, achieving 90.29 % RhB degradation, significantly outperforming Cu_2Cr-LDH/TiO_2 (56.45%) and pure Cu_2Cr-LDH (31.36%). This enhanced efficiency is attributed to the formation of a heterojunction between Cu_2Cr-LDH and BiOCl, which facilitates effective separation and transfer of charge carriers. The improved photocatalytic activity is primarily attributed to the well-dispersed BiOCl phase on the Cu_2Cr-LDH surface, demonstrating that interfacial architecture plays a more critical role than simply increasing the Bi or Ti content. Hydroxyl radicals and holes were determined to be the primary active species responsible for the degradation process. Additionally, both nanocomposites demonstrated remarkable stability and reusability, retaining high catalytic efficiency over four consecutive cycles. A detailed photocatalytic mechanism was proposed to explain the enhanced activity of the nanocomposites, highlighting the synergistic effects of the heterojunction structure and efficient charge carrier dynamics.

*Corresponding author Tel.: +21 3781487204
E-mail: alialiboutaiba@gmail.com
DOI: 10.22104/aet.2026.7739.2177
COPYRIGHTS: ©2026 Advances in Environmental Technology (AET). This article is an open access article distributed under the terms and conditions of the Creative Commons Attribution 4.0 International (CC BY 4.0) (https://creativecommons.org/licenses/by/4.0/)

1. Introduction

The release of industrial effluents containing non-biodegradable organic dyes from industries such as textiles, paper, leather, plastics, pharmaceuticals, and food production has become a critical environmental concern. These dyes, even in trace amounts, can have detrimental effects on aquatic ecosystems. They hinder photosynthetic activity by blocking sunlight penetration, which is essential for the survival of aquatic plants and algae. Additionally, the increased toxicity levels from these dyes can harm aquatic organisms, disrupt ecosystems, and compromise water quality. To combat these adverse effects, it is imperative to develop and implement effective treatment strategies that can efficiently remove or degrade these pollutants, thereby safeguarding aquatic life and maintaining ecological balance. Advanced treatment methods, including photocatalytic degradation, adsorption, and advanced oxidation processes, are being explored to address this pressing issue and reduce the environmental footprint of industrial activities [1].

Consequently, there is a growing demand for cost-effective and efficient methods to eliminate these harmful pollutants. Among the advanced strategies explored, photocatalytic oxidation stands out as a promising and efficient technology for degrading a wide range of pollutants using light energy [2,3]. Harnessing solar energy, a clean, renewable, and cost-free power source, has been extensively studied to drive this process [4]. However, the effectiveness of photocatalytic materials under solar irradiation is often limited due to issues like electron-hole recombination and insufficient absorption of sunlight [5].

To overcome these challenges, researchers are focusing on developing innovative photocatalysts that exhibit high activity and sensitivity to visible light. Semiconductor photocatalysts, in particular, have shown significant potential for solar energy conversion and pollutant degradation. Among the many studied materials, BiOCl and TiO_2 have attracted considerable attention due to their unique properties and catalytic applications [6, 7]. However, earlier studies revealed that the pure phases of BiOCl and TiO_2 have limited photocatalytic performance under solar light, which restricts their practical applications [8, 9]. To improve the efficiency of these materials, various strategies have been employed, such as doping with metallic and non-metallic elements, to enhance optical absorption and promote the separation of charge carriers. These approaches aim to improve the overall performance of photocatalysts, making them more effective for environmental remediation and pollution control [10-12].

Another class of materials that has garnered significant attention in catalysis is layered double hydroxides (LDHs). These materials are noted for their high anion exchange capacity, large specific surface area, non-toxicity, low cost, and straightforward synthesis method [13]. Layered double hydroxides, commonly referred to as anionic clays, have a general formula of $[M^{2+}(1–X)M^{3+}(X)(OH)_2]^{X+}(A^{n-})^{X/n}.mH_2O$. In this formula, M^{2+} and M^{3+} represent the bivalent and trivalent cations, respectively, while A^{n-} denotes the interlayer anions and m indicates the number of water molecules in the layered structure. This composition results in positively charged layers that are balanced by the intercalation of hydrated anions [14]. LDHs can be regarded as semiconductors due to their distinct layered structure and versatile chemical composition. While LDHs are extensively used for pollutant adsorption and catalysis, potentially enhancing catalytic reaction efficiency by improving pollutant adsorption and hydroxyl radical (OH·) production, they exhibit limited photocatalytic activity. This is due to issues such as poor charge carrier mobility, rapid recombination of charge carriers, and inefficient electron-hole transfer [15, 16]. For example, the photocatalytic activity of pure NiFe-LDH showed a low degradation efficiency, with only 39% of RhB degraded in 240 minutes under visible light irradiation [17] and, in another study, only 29.8% of RhB dye was degraded by NiFe-LDH in 120 minutes. Additionally, LDHs can be used as a support material due to their well-organized and tunable functional characteristics, allowing for precise structural modifications. Furthermore, the surface of LDHs contains numerous alkaline coordination sites, making them highly suitable for anchoring transition metal atoms and creating highly active catalytic centers, as the study

indicated. After surface modification with BiOCl, the BiOCl-NiFe-LDH composite demonstrated a higher color removal efficiency than NiFe-LDH. Recently, assembling LDHs nanosheets onto a photosensitive substrate to create heterostructure arrays has emerged as an efficient approach to enhance the exposure of active sites and promote the separation and transfer of photogenerated carriers, and in terms of energy structure, the charge transfer processes within the formed heterostructures generally occur across staggered band gaps [12].

Several reports have been published on LDH-based semiconductor materials for photocatalytic degradation of dyes, such as ZnCr-LDH surfaces decorated with TiO_2 and BiOCl used in the photodegradation of RhB [18, 19]. AgCl-BiOCl-NiFe-LDH composite photocatalysts have been synthesized and tested for their efficiency under visible light. The photocatalytic performance of these composites was evaluated through the degradation of RhB dye. Results demonstrated that the composite catalysts achieved 97.8 % degradation of RhB within just one hour of visible light exposure [20]. NiCr-LDH-based photocatalysts show great potential in the field of photocatalysis, particularly for harnessing solar energy to drive chemical processes. These catalysts are highly effective for the oxidation of organic pollutants and the generation of renewable energy. Their layered structure facilitates efficient charge separation and transfer, enhancing their overall photocatalytic performance. Additionally, NiCr-LDH photocatalysts are recognized for their durability and stability, making them a sustainable choice for various environmental remediation and energy production applications [21].

In addition to their high adsorption capacity across the spectral range, the metal-to-metal charge transfer (MMCT) in LDHs can be finely adjusted through isomorphous substitutions. This allows for precise tuning of the electronic properties, making LDH more versatile for various applications, as different metal ions can be substituted within the layered structure to enhance charge transfer dynamics and optimize their photocatalytic or adsorption performance [22]. The enhancement of the intrinsic properties of LDH is strongly influenced by the choice of cations that constitute the layers. By carefully selecting and varying the type and ratio of divalent and trivalent cations in the layered double hydroxide structure, it is possible to fine-tune their chemical, thermal, and catalytic properties. This cationic substitution allows for modifications in the material's electronic structure, surface area, charge density, and anion exchange capacity, making Layered double hydroxide highly adaptable for specific applications in environmental remediation, a study was conducted to investigate the effects of divalent metal ions on the photocatalytic properties of layered double hydroxides by varying the M^{II} metal ions while keeping the M^{II}/Cr^{III} atomic ratio constant at 2:1. The LDH containing cobalt showed the highest photocatalytic activity, achieving 90% removal of MO within 3 hours under solar light irradiation. The study further revealed, through optical difference spectra, that absorption in the visible region was due to metal-to-metal charge transfer (MMCT) excitation of oxo-bridged bimetallic linkages between M^{II}-O-Cr^{III} in neighboring MO_6 octahedra. This MMCT excitation in the visible range was identified as a key factor contributing to the enhanced degradation of MO [23]. Particularly, LDHs containing Cu are widely used in a variety of catalytic domains owing to their unique structural characteristics and the promising catalytic activity of the Cu atom. Moreover, Cu^{2+} served as the divalent cation to enhance the formation of defects while Cr^{3+} demonstrated high visible light absorption [24]. Among the prospective transition metals, the Cr^{3+} cation has a special electronic configuration, which enhances charge transfer and electron capture [25]. Based on the literature review, Cu_2Cr-LDH owns a low bandgap that enables simple electron-hole separation under visible light [23]. However, poor mobility of the charge carriers and fast recombination of the generated electron-hole occur, which is the major bottleneck that restricts the application of LDHs as photocatalysts [26]. On the other hand, the significant feature of LDHs is the plethora of combinations of various compounds that can be implemented in the LDH structure. Enhancing the separation rate of electron-hole pairs forms a heterostructure between the Layered double hydroxide's surface and semiconductors. TiO_2 and BiOCl nanoparticles

offer a cost-effective alternative for developing active catalysts, characterized by their high stability and recyclability through simple filtration processes.

This study focuses on the synthesis and characterization of two nanocomposite materials, Cu_2Cr-LDH/BiOCl and Cu_2Cr-LDH/TiO_2, to evaluate their photocatalytic performance in degrading Rhodamine B (RhB) under direct sunlight. The morphological, structural, and optical properties of these materials were thoroughly analyzed to understand their functional capabilities. The photocatalytic efficiency was assessed by examining key parameters, such as adsorbent dose, acidity of the dye solution, and reaction time. Furthermore, a detailed mechanism for the degradation of RhB using these composites was proposed, shedding light on the underlying processes that enhance their photocatalytic activity.

2. Materials and methods

The reagents used in this study included Copper (II) nitrate hexahydrate $Cu(NO_3)_2{\cdot}6H_2O$ (99%), Chromium (III) nitrate nonahydrate $Cr(NO_3)_3{\cdot}9H_2O$ (99%), sodium hydroxide NaOH (99%), sodium chloride NaCl (99%), hydrochloric acid HCl (36%), sodium carbonate Na_2CO_3 (99%), ethanol (99.97%), diethylene glycol (99.95%), and Rhodamine B. All of these were procured from Biochem-Chemo Pharma. Additionally, tetrabutyl titanate ($C_{16}H_{36}O_4Ti$) (97%), Bismuth (III) nitrate pentahydraté $Bi(NO_3)_3{\cdot}5H_2O$ (99%), Ethylenediaminetetraacetic acid disodium salt dihydrate $C_{10}H_{14}N_2Na_2O_8 \cdot 2H_2O$ (Na2EDTA, 99.995% purity) were procured from Sigma-Aldrich. Ascorbic acid $C_6H_8O_6$ (99.7 %) was obtained from Merck/SRL.

The characterization techniques used in this research work included the following: D/MAX-RB X-ray powder diffraction (XRD, Rigaku) with CuKα radiation (λ= 0.15405 nm) at 40 KV and 30 mA, UV-Vis spectrometer (JASCO V750) Shimadzu, field emission scanning electron microscope (BRUKER; JEOL, Qunta 250) at 20-12.5 keV, and X-ray photoelectron spectroscopy (Kratos Nova) with an Al Kα line (1486.6 eV) radiation. Cu_2Cr-LDH (molar ratio 2:1) was synthesized via co-precipitation at pH 10, followed by hydrothermal treatment at 80 °C for 24 h. The Cu_2Cr-LDH/TiO_2 nanocomposites were obtained by dispersing Cu_2Cr-LDH in ethanol with tetrabutyl titanate, then hydrothermally treating at 180 °C for 24 h. The Cu_2Cr-LDH/BiOCl nanocomposites were prepared through a two-step process using $Bi(NO_3)_3{\bullet}5H_2O$ and NaCl solutions, followed by hydrothermal treatment at 180 °C for 12 h. TiO_2 was synthesized from tetrabutyl titanate in ethanol, hydrothermally treated at 180 °C for 24 h, and dried; BiOCl was synthesized using the same procedure as Cu_2Cr-LDH/BiOCl but without LDH [23].

The photocatalytic activity was tested under sunlight using 0.1 g of the catalyst in 50 mL of RhB solution (5 mg/L, pH 7, 25 °C). After 30 min dark equilibration, the suspension was irradiated, and aliquots were collected at intervals, centrifuged, and analyzed with a HACH DR 5000 spectrophotometer. Dye degradation efficiency was then calculated [27]:

$$R\% = \frac{(C_0 - C_t)}{C_0} \times 100 \quad (1)$$

where c_o (mg/L) is the initial concentration, and c_t (mg/L) is the concentration at time t (min).

Scavenger experiments were performed to investigate the active species generated in the photocatalytic system, consisting of a photocatalyst, RhB, Cu_2Cr-LDH/BiOCl, and Cu_2Cr-LDH/TiO_2 under sunlight. Ethylenediaminetetraacetic acid (EDTA-2Na, 10 mM), Ascorbic acid (1 mM), and Ethanol (10 mM) were used as scavengers, introduced into the photocatalytic system in the amount of 1 ml to capture holes ($h^{\bullet}$), superoxide radicals ($^{\bullet}O_2^-$), electrons (e^-), and hydroxyl radicals ($OH^{\bullet}$), respectively.

3. Results and discussion

Figure 1 displays the XRD patterns of the synthesized materials. The XRD pattern of Cu_2Cr-LDH shows distinct peaks at (003), (006), (012), (015), (018), (110), and (113), confirming its layered LDH structure. These reflections match the 3R rhombohedral symmetry (Figure S1) [28]. XRD analysis confirmed the phase purity of BiOCl and TiO_2, with diffraction peaks matching standard reference patterns (Figure S2) [19].

The nanocomposites (Cu_2Cr-LDH/TiO_2 and Cu_2Cr-LDH/BiOCl) (Figure. 1) retained the hydrotalcite structure, though some structural modifications were observed. For Cu_2Cr-LDH/TiO_2, reduced crystallinity, lattice expansion, and larger particle size (11.85 nm) indicated structural distortions from TiO_2 incorporation. In Cu_2Cr-LDH/BiOCl, distinct BiOCl peaks confirmed successful integration, though the reduced intensity of LDH peaks suggested partial disruption of the layered structure. Overall, XRD results demonstrate effective composite formation with TiO_2 and BiOCl phases [29, 30]. The UV-Vis diffuse reflectance spectra (Figure 2) of Cu_2Cr-LDH show three absorption regions: 200-300 nm - ligand-to-metal charge transfer (O 2p → Cu/Cr 3d t_2g), 300-500 nm – d–d transitions of Cu^{2+} and Cr^{3+} in octahedral fields (t_2g → e g), These transitions highlight the role of the oxo-bridged Cu–Cr LDH system as a photoactive center, where Cu^{2+} ions (partially filled 3d orbitals) enhance photocatalytic activity.

The Cu_2Cr-LDH/TiO_2 nanocomposite retained similar bands but displayed an additional strong absorption at 315 nm (O2p → Ti3d t_2g), confirming TiO_2 incorporation. In contrast, Cu_2Cr-LDH/BiOCl exhibited a weaker band at 307 nm, linked to Cl3p → Bi6p transitions, evidencing BiOCl integration into the LDH structure [33].

A semiconductor can be distinguished from other materials by its band gap energy, which is calculated using the following equation [31]:

$$(\alpha h\nu)^{\frac{1}{n}} = A\left(h\nu - E_g\right) \quad (2)$$

In this equation, α represents the absorption coefficient, h is Planck's constant, υ denotes the frequency of the incident light, A is a proportionality constant, and Eg corresponds to the band gap energy of the semiconductor. According to Tauc's relation, the parameter n indicates the nature of the optical transition in the material (n=1/2 for direct transitions and n=2 for indirect transitions).

The band gap energy (Eg) can be determined by extending the linear section of the curve to the energy axis. Based on Figure 2 (b), the estimated band gap energies for Cu_2Cr-LDH, Cu_2Cr-LDH/TiO_2, Cu_2Cr-LDH/BiOCl, TiO_2, and BiOCl were found to be 2.5 eV, 1.54 eV, 2.3 eV, 3.1 eV, and 3.32 eV, respectively. The valence band (E_{VB}) and conduction band (E_{CB}) energies of a semiconductor are calculated using the following equations [32]:

$$E_{(VB)} = \chi - E^e + \frac{1}{2}E_g \quad (3)$$

$$E_{(CB)} = E_{(VB)} - E_g \quad (4)$$

In these equations, χ represents the absolute electronegativity of the semiconductor, and_E^e denotes the potential energy of free electrons on the standard hydrogen scale (approximately 4.5 eV). The calculated parameters are summarized in Table 1.

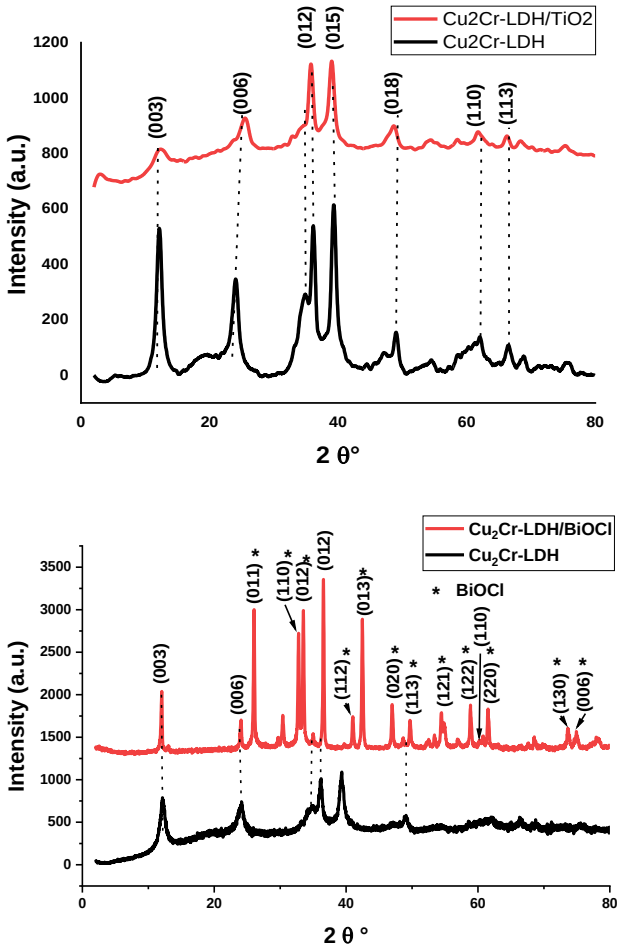

Fig. 1. X-ray diffractograms of Cu_2Cr-LDH/TiO_2 and Cu_2Cr-LDH/BiOCl.

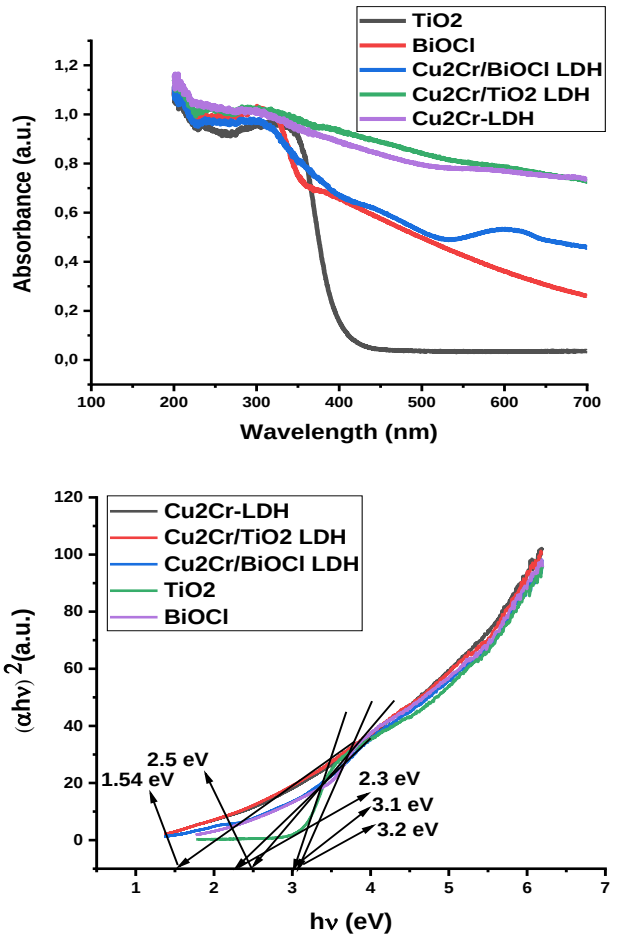

Fig. 2. (a) UV-Vis diffuse reflectance spectra of the synthesized photocatalysts; (b) Bandgap energy estimations for the materials.

XPS analysis was conducted to evaluate the elemental composition and oxidation states of the synthesized materials.

The full XPS survey spectrum of the Cu_2Cr/BiOCl nanocomposite, shown in Figure 3 (a), confirmed the presence of Cu, Cr, C, Bi, Cl, and O elements. Figure. 3 (b), XPS analysis, confirmed Cu^{2+} in $[CuO_6]$ octahedral coordination (Cu 2p peaks at 932.7, 952.3 eV), The absorption band in the 500-700 nm - metal-to-metal range is attributed to metal-to-metal charge transfer (Cu^{2+}–O–Cr^{3+} → Cu^{+}–O–Cr^{4+}) [34].

Table 1. Photophysical properties of prepared materials.

Materials	Eg (eV)	χ	$E_{(VB)\,(V/SNH)}$	$E_{(CB)\,(V/SNH)}$
Cu_2Cr-LDH	2.5	7.194	3.944	1.444
Cu_2Cr-LDH/TiO_2	1.54	-	-	-
Cu_2Cr-LDH/BiOCl	2.3	-	-	-
TiO_2	3.1	5.639	2.689	-0.411
BiOCl	3.32	6.12	3.28	0.023

Cr^{3+} states (577, 986.2 eV). The O 1s peak (531.53 eV) indicated hydroxyl groups, while C 1s peaks (284.5, 288.3 eV) corresponded to surface carbon and interlayer carbonate [35].

XPS confirmed Ti^{4+} in Cu_2Cr-LDH/TiO_2, with Ti 2p peaks at 458.3 and 464.6 eV and satellite features at 461.8 and 466.7 eV. O 1s peaks at 529.4 and 532.4 eV indicated lattice oxygen and surface –OH groups, confirming anatase TiO_2 incorporation (Figure S3) [36].

XPS spectra of Cu_2Cr-LDH/BiOCl revealed Bi 4f peaks (158.9, 164 eV), Cl 2p peaks (197.9, 199.4 eV), and O 1s peaks (529.8, 531.6, 532.6 eV). These are attributed to Bi–O bonds, Cl–O bonds, and OH groups, confirming the successful integration of BiOCl in the composite [37].

SEM images (Figure 4) highlight the morphology of TiO_2, BiOCl, and their Cu_2Cr-LDH-based nanocomposites. TiO_2 shows uniform pseudo-spherical nanoparticles (50–100 nm), typical of well-crystallized structures with high surface area. Cu_2Cr-LDH/TiO_2 exhibits plate-like LDH layers decorated with dispersed TiO_2 nanoparticles, confirming successful composite formation. BiOCl displays stacked nanosheets with smooth surfaces and ~39 nm thickness, consistent with its layered crystalline nature. In Cu_2Cr-LDH/BiOCl, irregular nanosheet aggregation and BiOCl nanoflowers integrated within the LDH structure form a hierarchical morphology. This combination enhances surface area, stability, and the density of active sites, improving photocatalytic and adsorption performance.

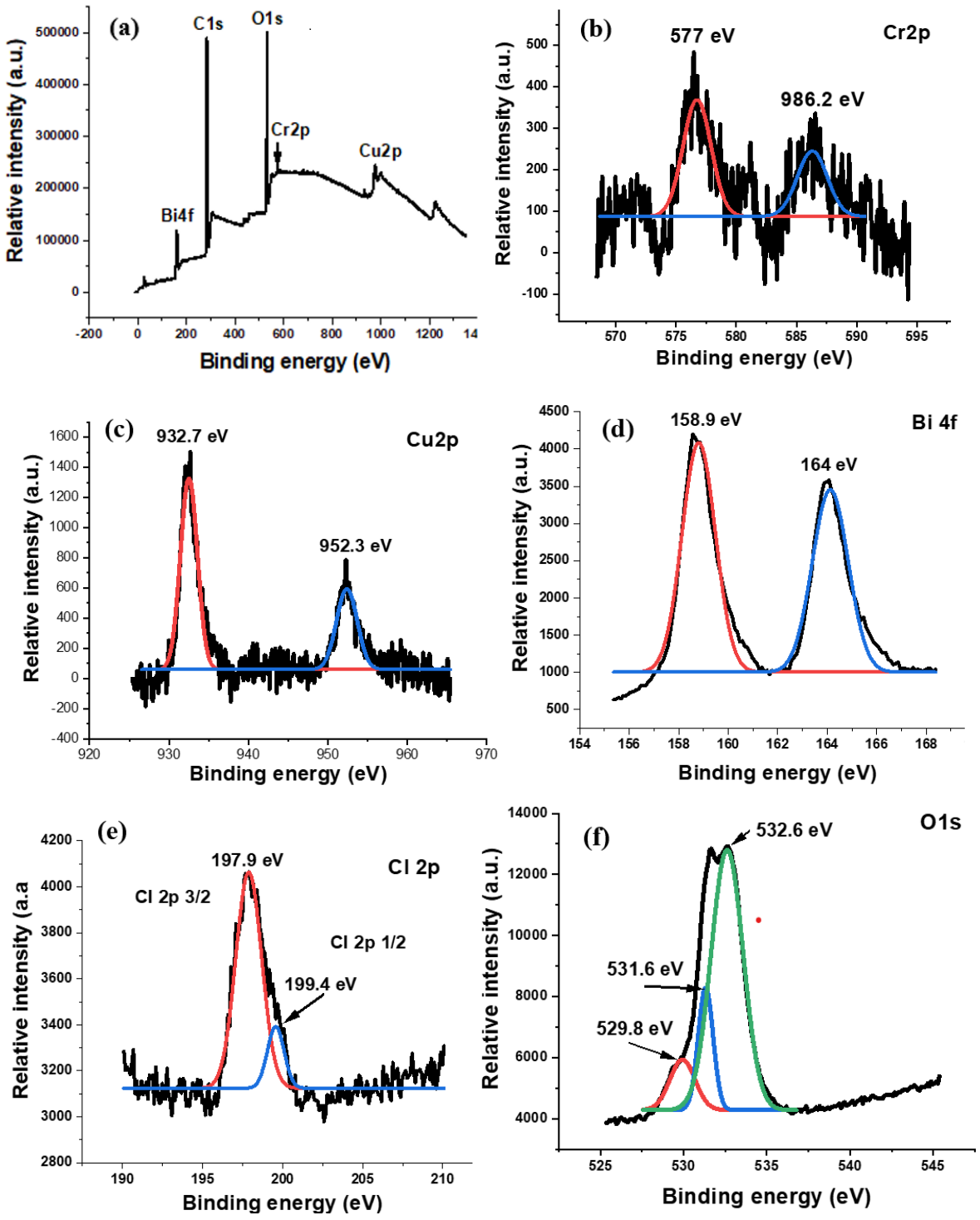

Fig. 3. (a)XPS Spectra for Cu_2Cr-HDL/BiOCl, with high resolution XPS spectra for (b) Cr 2p, (c) Cu 2p, (d) Bi 4f, (e) Cl 2p, and (f) O 1s.

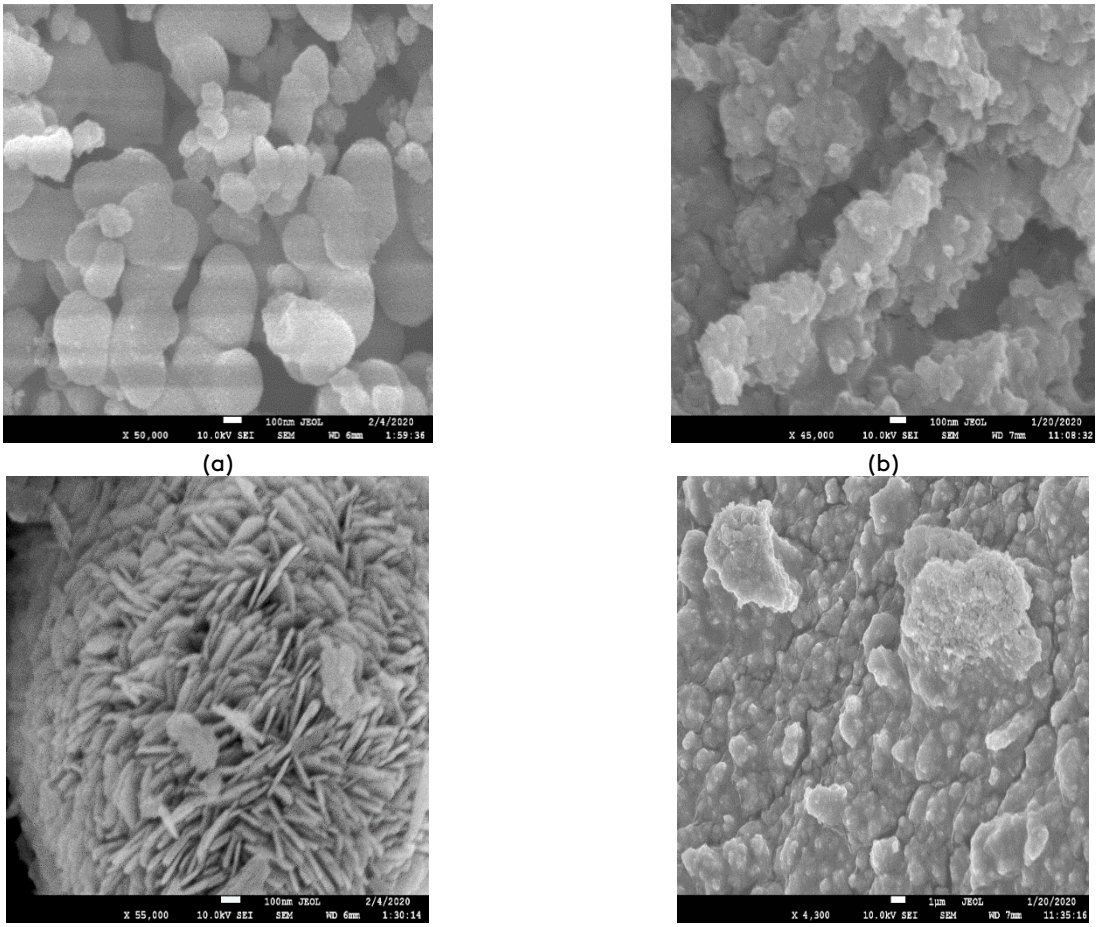

Fig. 4. Scanning electron microscopy (SEM) images of (a) TiO_2, (b) Cu_2Cr-LDH/TiO_2, (c) BiOCl, and (d) Cu_2Cr-LDH/BiOCl.

3.1. Photocatalytic performance

The photocatalytic activity of the catalysts was assessed by rhodamine B degradation under sunlight. Blank tests showed 15.7% self-degradation, while adsorption in dark conditions was limited, with BiOCl (28.67%) showing the highest uptake and TiO_2 almost negligible. After 60 minutes of irradiation, BiOCl and TiO_2 exhibited the highest efficiencies at 96.45% and 70.22%, respectively, followed by Cu_2Cr-LDH/BiOCl (90.29%), Cu_2Cr-LDH/TiO_2 (45.69%), and bare Cu_2Cr-LDH (36.81%). The superior performance of the composites is attributed to heterojunction formation, improved morphology, and interfacial charge transfer, which effectively suppressed electron–hole recombination. Furthermore, the photocatalytic activities of BiOCl, TiO_2, and the composites Cu_2Cr-LDH/BiOCl and Cu_2Cr-LDH/TiO_2 are not solely dependent on their Bi or Ti content. The higher activity of BiOCl or TiO_2 in the composite form (despite the lower amount compared to the pure phases) is attributed to the increased specific surface area of these nanophases dispersed on the Cu_2Cr-LDH layers, which enhances light absorption and promotes more efficient separation of photo-induced electron–hole pairs.

The photocatalytic degradation kinetics of RhB can be analyzed using the pseudo-first-order kinetic model, expressed as [18]:

$$\ln (C_0 / C_t) = kt \quad (6)$$

Here, C_0 denotes the initial concentration of RhB, Ct represents the concentration of RhB at time t, and k is the apparent rate constant (min^{-1}). This model is commonly employed to describe the degradation behavior of organic pollutants under photocatalytic conditions. As illustrated in Figure 5 (b), the photocatalytic activity of Cu_2Cr-LDH/TiO_2 and Cu_2Cr-LDH/BiOCl nanocomposites for RhB degradation significantly surpassed that of the pure Cu_2Cr-LDH phase. This model is commonly

employed to describe the degradation behavior of organic pollutants under photocatalytic conditions. The findings are presented in Figure 6 and Table 2. As illustrated in Figure 6 (b) and summarized in Table 2, the photocatalytic activity of Cu_2Cr-LDH/TiO_2 and Cu_2Cr-LDH/BiOCl nanocomposites for RhB degradation significantly surpassed that of the pure Cu_2Cr-LDH phase.

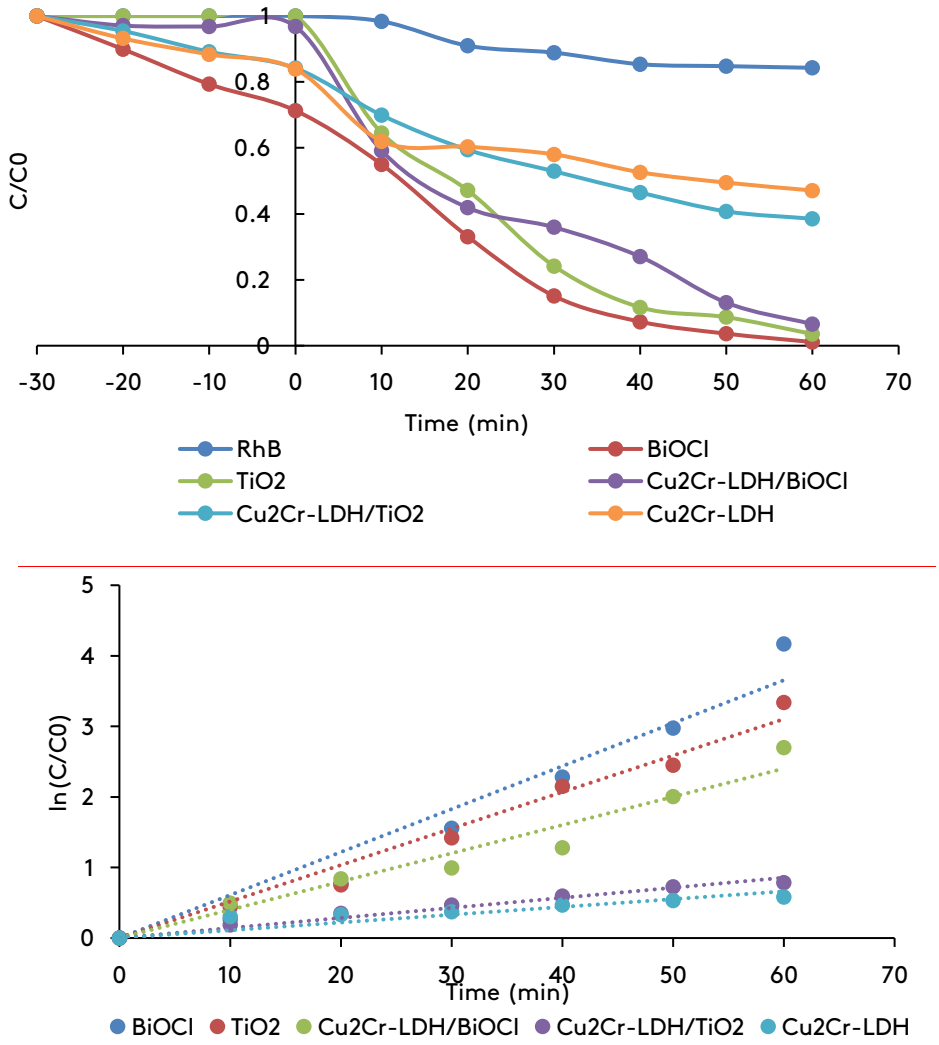

Fig. 5. (a) Temporal variation in the relative concentration of RhB dye; (b) Plots of $\ln(C/C_0)$ as a function of degradation time.

Table 2. Photocatalytic degradation kinetic of RhB by various materials.

Material	R_{Ad}, (%)	R_{ph}, (%)	K_{app}, (min^{-1})	$t_{1/2}$, (min)	$V_0 * 10^{-3}$, (mg/L min^{-1})	R^2
Rhodamine B	-	15.7	-	-	-	-
TiO_2	0	96.45	0.0517	11.379	1.84	0.98
BiOCl	28.67	70.22	0.0609	13.404	6.74	0.99
Cu_2Cr-HDL	16.11	36.81	0.011	17.325	5.1	0.95
Cu_2Cr-HDL/ TiO_2	16.11	45.69	0.0143	48.416	5.5	0.99
Cu_2Cr-HDL/ BiOCl	3.18	90.29	0.04	63	2.6	0.98

Figure 6 (b) clearly indicates a reduction in the rate constant k from Cu_2Cr-LDH/BiOCl to Cu_2Cr-LDH/TiO_2, suggesting that the modification of Cu_2Cr-LDH with BiOCl enhances its photocatalytic performance under sunlight. This improvement can be attributed to the unique morphology of BiOCl when deposited on the LDH surface, as well as the efficient generation and separation of electron-hole pairs on the photocatalyst's surface. These factors collectively contribute to the enhanced degradation efficiency of Rhodamine B.

pH is a critical factor affecting the efficiency of heterogeneous photocatalytic degradation of pollutants, as illustrated in Figure 6.

The effect of pH on RhB degradation was studied at pH 4, 7, and 10 using 5 ppm dye and 0.1 g catalyst. Carbonate-based LDH showed poor activity (45.69% at pH 7, 39.1% at pH 10), while Cu_2Cr-LDH/BiOCl achieved 90.29% at pH 7 and 94.4% at pH 10, indicating optimal performance in alkaline conditions. The results highlighted the strong influence of surface charge on photocatalysis [38-40].

At low pH, electrostatic repulsion between cationic RhB, protons, and the positively charged catalyst surface inhibited adsorption and photocatalytic activity. As pH increased, reduced repulsion enhanced adsorption and degradation efficiency [41-44].

3.2. Regeneration

Regeneration tests were performed to evaluate the reusability of Cu_2Cr-LDH/TiO_2 and Cu_2Cr-LDH/BiOCl nanocomposites. After each cycle, the catalysts were recovered, cleaned, and reused under identical conditions. As shown in Figure 7, both materials retained high photocatalytic activity over four cycles: Cu_2Cr-LDH/TiO_2 maintained ~54% efficiency, while Cu_2Cr-LDH/BiOCl achieved ~90% RhB degradation after 60 minutes. The stable performance confirms strong structural integrity and interfacial stability of the composites. Their reusability demonstrates excellent durability, making them cost-effective and promising candidates for large-scale environmental remediation. Although BiOCl exhibits the highest intrinsic photocatalytic performance, the use of composites such as Cu_2Cr-LDH/BiOCl or TiO_2-based systems is not solely aimed at enhancing photocatalytic activity, but also at increasing the practical applicability of the material in real water treatment processes. Indeed, BiOCl (39 nm) and TiO_2 (100 nm) nanoparticles tend to strongly agglomerate and are difficult to separate from treated water due to their very small size, which significantly limits their reusability and leads to a gradual loss of the photocatalyst over multiple cycles.

By supporting BiOCl (or TiO_2) in a nanostructured form on the Cu_2Cr-LDH layers, larger and more stable hierarchical particles are obtained, facilitating easy recovery through sedimentation or centrifugation without the need for complex filtration steps.

3.3. Effect of different scavengers

Scavenger experiments were conducted to identify the active species in RhB photodegradation by Cu_2Cr-LDH/BiOCl and Cu_2Cr-LDH/TiO_2 under sunlight. Results showed that holes (h^+) and hydroxyl radicals (•OH) were the dominant species, as their scavenging significantly reduced degradation efficiency. In contrast, superoxide radicals ($O_2•^-$) played a minor role, with only slight decreases observed upon scavenging.

The Cu_2Cr-LDH/BiOCl nanocomposite demonstrated higher efficiency than Cu_2Cr-LDH/TiO_2 due to its larger surface area and superior charge separation. Overall, these findings highlight the crucial role of h^+ and •OH in pollutant degradation and underline the potential of these nanocomposites for environmental remediation, Figure 8 (a) and 8 (b). Na_2EDTA, a scavenger for holes (h+), was introduced, and the degradation efficiency of RhB decreased significantly. For the Cu_2Cr-LDH/BiOCl nanocomposite, the decolorization rate dropped to 58.23% after 60 minutes of irradiation, while for Cu_2Cr-LDH/TiO_2, it fell to 33.19 %. This substantial reduction indicates that holes (h^+) play a crucial role in the photocatalytic process, likely by directly oxidizing RhB molecules or generating other reactive species.

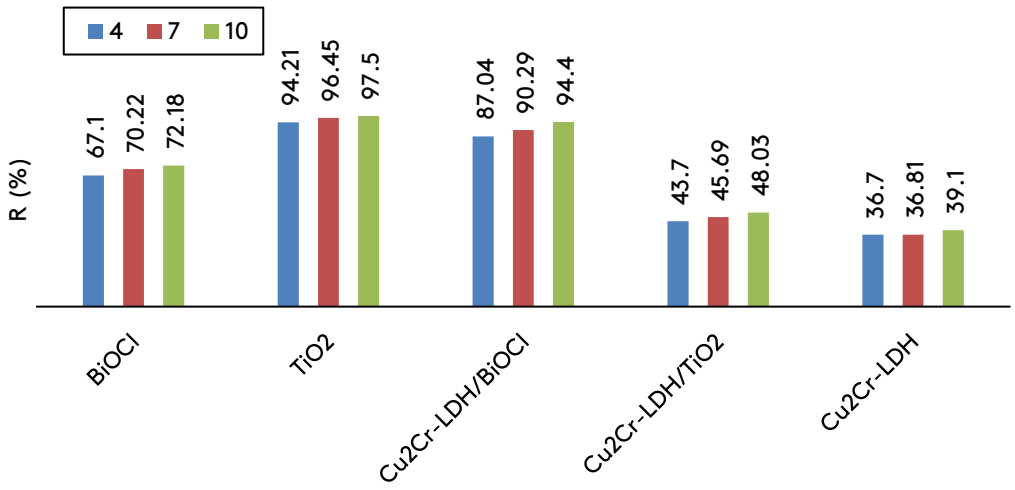

Fig. 6. Effect of solution pH on the degradation efficiencies.

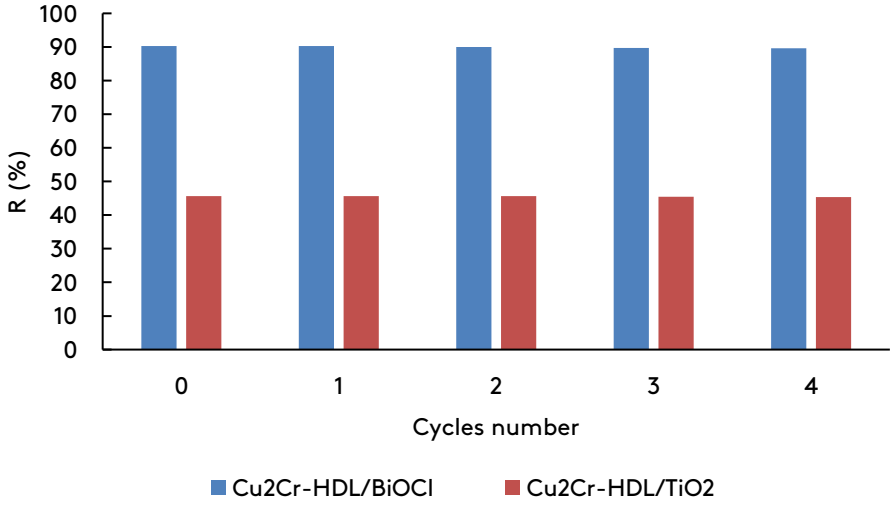

Fig. 7. Reusability tests for the photocatalytic degradation of Rhodamine B under sunlight irradiation.

Similarly, the addition of ethanol, which scavenges hydroxyl radicals (HO•), resulted in a reduction of the degradation efficiency to 46.34% for Cu_2Cr-LDH/BiOCl and 24.09% for Cu_2Cr-LDH/TiO_2.

This suggests that HO• radicals are also significant contributors to the degradation process, as they are highly reactive and can effectively break down organic pollutants. In contrast, when ascorbic acid, a scavenger for superoxide radicals ($^{-}O_2$•), was used, the degradation efficiency remained relatively high, with Cu_2Cr-LDH/BiOCl achieving 87.45% and Cu_2Cr-LDH/TiO_2 reaching 43.87% under the same irradiation conditions.

This indicates that superoxide radicals ($^{-}O_2$•) have a lesser role in the photodegradation process compared to holes (h^+) and hydroxyl radicals (HO•). These results demonstrate that the presence of Na_2EDTA, ethanol, and ascorbic acid significantly delayed the photocatalytic degradation of RhB, indicating that holes (h^+) and hydroxyl radicals (HO•) are the dominant active species driving the process. Superoxide radicals ($^{-}O_2$•) played a comparatively minor role in the degradation mechanism.

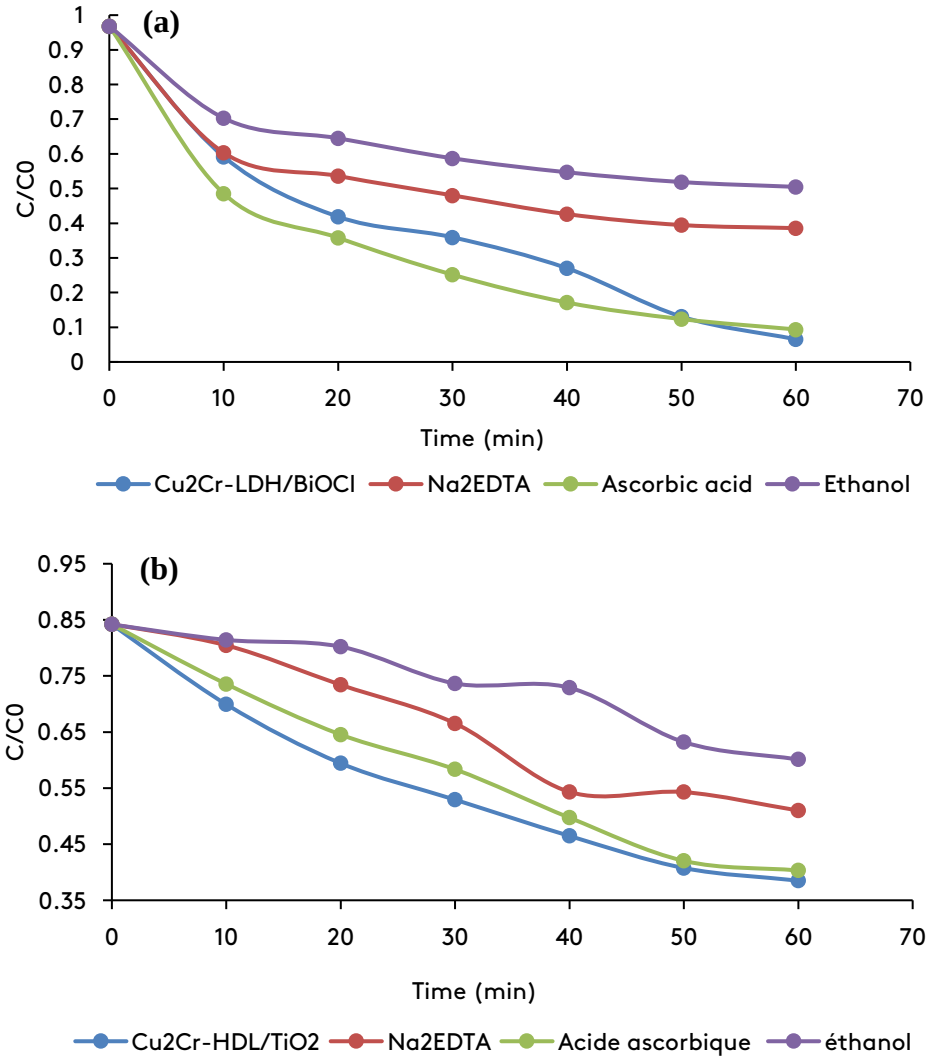

Fig. 8. The photocatalytic degradation of Rhodamine B by (a) Cu_2Cr-LDH/ BiOCl and (b) Cu_2Cr-LDH/TiO_2 with and without scavengers.

3.4. Photocatalytic degradation mechanism of RhB over the nanocomposites

The enhanced photocatalytic activity of Cu_2Cr-LDH/BiOCl under sunlight arises from the synergistic effects of its heterojunction structure and the Metal-to-Metal Charge Transfer (MMCT) process. Upon irradiation, both semiconductors are photoexcited, generating electron-hole pairs. Charge transfer occurs bidirectionally: electrons migrate from the CB of BiOCl to Cu_2Cr-LDH, while holes move from Cu_2Cr-LDH to BiOCl. This reduces recombination and enhances charge separation. In BiOCl, holes possess sufficient potential to oxidize H_2O/OH^- into highly reactive •OH radicals, which play a dominant role in RhB degradation. Although electrons in Cu_2Cr-LDH's CB cannot reduce O_2 to $O_2\bullet^-$, RhB self-photosensitization provides an additional pathway [44]: excited RhB electrons transfer sequentially to BiOCl and Cu_2Cr-LDH, and directly reduce O_2 to $O_2\bullet^-$. These ROS, together with •OH, ensure efficient RhB mineralization (Scheme 1).

For Cu_2Cr-LDH/TiO_2, the mechanism is similar but less efficient: TiO_2's VB cannot oxidize H_2O to •OH (only OH^-), while its CB electrons can reduce O_2 to $O_2\bullet^-$. Consequently, fewer •OH radicals are generated compared to BiOCl-based systems. Scavenger studies confirm that holes (h^+) and •OH are the primary active species, while $O_2\bullet^-$ plays a secondary role.

Overall, the Cu_2Cr-LDH/BiOCl heterostructure demonstrates superior performance due to more

favorable band alignment, efficient charge transfer, and RhB-assisted self-photosensitization.

3.5. Comparison of proposed nanostructures with other photocatalysts

In Table 3, the proposed photocatalyst is compared with other photocatalysts for RhB degradation [8, 10, 12, 28]. The CuCr-LDH/BiOCl nanostructure can remove more RhB with less photocatalyst consumption in a shorter time under visible light and is comparable with other photocatalysts.

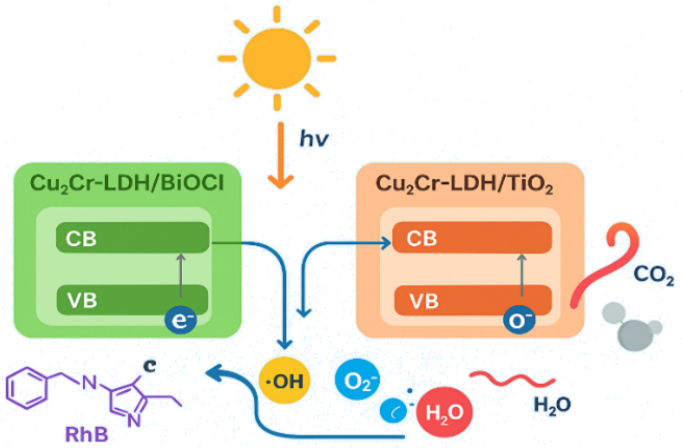

Scheme 1. Mechanism of Rhodamine B dye degradation using Cu_2Cr-LDH/BiOCl nanocomposites.

Table 3. Comparison of proposed photocatalyst with other photocatalysts.

Photocatalyst	Concentration (ppm)	Photocatalyst Amount (g)	Time (min)	Photocatalytic efficiency (%)	Ref
$BiOCl/TiO_2$	20	0.8	80	99	[8]
Sn-doped BiOCl	10	20	60	91.2	[10]
NiFe–LDH/BiOCl	20	0.5	60	93.3	[12]
ZnCrLDH/graphene	10	0.1	140	93	[28]
Cu_2Cr-LDH/BiOCl	5	0.1	60	90.29	Present work
Cu_2Cr-LDH/TiO_2	5	0.1	60	56.45	Present work
Cu_2Cr-LDH	5	0.1	60	31.36	Present work

4. Conclusion

Nano-heterostructured Cu_2Cr-LDH/BiOCl and Cu_2Cr-LDH/TiO_2 composites were successfully synthesized via co-precipitation and hydrothermal methods, with controlled molar ratios of Cu^{2+}/Cr^{3+} (2:1) and Cr^{3+}/Bi^{3+} or Cr^{3+}/Ti^{4+} (2:2).

Structural and optical characterizations (XRD, SEM, UV–vis, XPS) confirmed the formation of well-defined heterojunctions, and the photocatalytic activity was assessed through Rhodamine B (RhB) degradation under sunlight. The photocatalytic efficiency followed the trend Cu_2Cr-LDH/BiOCl > Cu_2Cr-LDH/TiO_2 > Cu_2Cr-LDH, mainly due to the effective heterojunction-induced charge separation and reduced electron–hole recombination, further enhanced by RhB self-photosensitization.

Scavenger experiments demonstrated that holes (h^+) and hydroxyl radicals (•OH) are the primary reactive species governing the degradation mechanism. In addition, the composites exhibited high stability and reusability over four recycling cycles. Overall, these findings highlight the great potential of Cu_2Cr-LDH-based heterostructures, particularly Cu_2Cr-LDH/BiOCl, as highly efficient and sustainable photocatalysts for real wastewater treatment applications.

Acknowledgements

The authors are grateful to the Laboratory of Chemistry of Inorganic Materials and Applications (LCMIA) and the University of Science and Technology of Oran Mohamed Boudiaf (USTO-MB) for providing laboratory and instrumentation facilities, as well as UV–Visible spectroscopic, XRD, and SEM analyses.

Author's contribution

Ali Bouteiba: Drafting original article, carrying literature study and reporting, assisting in technical content writing, formatting, generating artistic diagrams. Ali Bouteiba, Naceur Benhadria: Conceptualization, planning, reviewing. Nourredine Bettahar: drafting, formatting.

Conflict of interest

No potential conflict of interest was reported by the authors.

Data availability

Not Applicable.

Funding

Self-funded.

References

[1] Dutta, S., Adhikary, S., Bhattacharya, S., Roy, D., Chatterjee, S., Chakraborty, A., et al. (2024). Contamination of textile dyes in aquatic environment: Adverse impacts on aquatic ecosystem and human health, and its management using bioremediation. *J. Environ. Manage.*, *353*, 120103. https://doi.org/10.1016/j.jenvman.2024.120103

[2] Delcy, V. R., Naidu, S. M., Srihari, G., Umadevi, V., Balamurugan, K. S., Golkonda, S. R., et al. (2024). Influence of gadolinium substitution on the crystal structure of NiO and its maximized photocatalytic degradation activity on tetracycline and direct yellow pollutants. *Phys. B Condens. Matter*, *695*, 416546. https://doi.org/10.1016/j.physb.2024.416546

[3] Olatunde, O. C., Sawunyama, L., Yusuf, T. L., & Onwudiwe, D. C. (2024). Visible light driven $CuBi_2O_4$ heterostructures and their enhanced photocatalytic activity for pollutant degradation: A review. *J. Water Process Eng.*, *66*, 105890. https://doi.org/10.1016/j.jwpe.2024.105890

[4] Peng, H., Ji, C., Yang, R., L. Dong, & Zheng, X. (2024). $LaFeO_3/MgFe_2O_4$ hybrids for boosting the solar-light photocatalytic persulfate oxidation of tetracycline hydrochloride. *Colloids Surf. A Physicochem. Eng. Asp.*, *696*, 134340. https://doi.org/10.1016/j.colsurfa.2024.134340

[5] Perumal, V., Uthrakumar, R., Chinnathambi, M., Inmozhi, C., Robert, R., Rajasaravanan, M. E., et al. (2023). Electron-hole recombination effect of SnO_2-CuO nanocomposite for improving methylene blue photocatalytic activity in wastewater treatment under visible light. *J. King Saud Univ. Sci.*, *35*(1), 102388. https://doi.org/10.1016/j.jksus.2022.102388

[6] Wang, J., Wei, Y., Yang, B., Wang, B., Chen, J., & Jing, H. (2019). In situ grown heterojunction of Bi2WO6/BiOCl for efficient photoelectrocatalytic CO2 reduction. *J. Catal.*, *377*, 209–217. https://doi.org/10.1016/j.jcat.2019.06.007

[7] Sangeetha, M., Kalpana, S., Senthilkumar, N., & Senthil, T. S. (2024). Investigation on visible-light induced photocatalytic activity for pure, Ce:doped TiO2 and B:Ce co-doped TiO2 catalysts. *Optik*, *301*, 171687. https://doi.org/10.1016/j.ijleo.2024.171687

[8] Li, W., Tian, Y., Li, H., C. Zhao, B. Zhang, Zhang, H., et al. (2016). Novel $BiOCl/TiO_2$ hierarchical composites: Synthesis, characterization and application on photocatalysis. *Appl. Catal. A Gen.*, *516*, 81–89. https://doi.org/10.1016/j.apcata.2016.02.006

[9] Kavitha, S., Jayamani, N., & Barathi, D. (2021). Investigation on SnO2/TiO2 nanocomposites and their enhanced photocatalytic properties for the degradation of methylene blue under solar light irradiation. *Bull. Mater. Sci.*, *44*(1), 48. https://doi.org/10.1007/s12034-020-02291-4

[10] Zulkiflee, A., Khan, M. M., Khan, A., Khan, M. Y., Dafalla, H. D. M., & Harunsani, M. H. (2023). Sn-doped BiOCl for photoelectrochemical activities and

photocatalytic dye degradation under visible light. *Heliyon*, *9*(11), e21270. https://doi.org/10.1016/j.heliyon.2023.e21270

[11] Xie, T., Sun, S., Xu, J., Luo, Y., & Cui, J. (2022). Purposefully designing Co-S-codoping in hierarchical BiOCl architectures and elucidating the mechanism for enhanced visible-light-driven photocatalytic activity. *Appl. Surf. Sci.*, *604*, 154582. https://doi.org/10.1016/j.apsusc.2022.154582

[12] Ma, J., Ding, J., Yu, L., Li, L., Kong, Y., & Komarneni, S. (2015). BiOCl dispersed on NiFe–LDH leads to enhanced photo-degradation of Rhodamine B dye. *Appl. Clay Sci.*, *109-110*, 76–82. https://doi.org/10.1016/j.clay.2015.02.009

[13] Ali, B., Naceur, B., Abdelkader, E., Karima, E., & Nourredine, B. (2020). Competitive adsorption of binary dye from aqueous solutions using calcined layered double hydroxides. *Int. J. Environ. Anal. Chem.*, 1–20. https://doi.org/10.1080/03067319.2020.1766035

[14] Riaz, S., Rehman, A., Akhter, Z., Najam, T., Hossain, I., Karim, M. R., et al. (2024). Recent advancement in synthesis and applications of layered double hydroxides (LDHs) composites. *Mater. Today Sustain.*, *27*, 100897. https://doi.org/10.1016/j.mtsust.2024.100897

[15] Wu, Y., Wang, H., Sun, Y., Xiao, T., Wu, T., Yuan, X., et al. (2018). Photogenerated charge transfer via interfacial internal electric field for significantly improved photocatalysis in direct Z-scheme oxygen-doped carbon nitrogen/CoAl-layered double hydroxide heterojunction. *Appl. Catal. B Environ.*, *227*, 530–540. https://doi.org/10.1016/j.apcatb.2018.01.069

[16] Vennapoosa, C. S., Shelake, S. P., Jaksani, B., Jamma, A., Abraham, B. M., Sainath, A. V. S., et al. (2024). Surface engineering of a 2D CuFe-LDH/MoS2 photocatalyst for improved hydrogen generation. *Mater. Adv.*, *5*(10), 4159–4171. https://doi.org/10.1039/d3ma00881a

[17] He, Y., Zhou, S., Wang, Y., Jiang, G., & Jiao, F. (2021). Fabrication of g-C_3N_4@NiFe-LDH heterostructured nanocomposites for highly efficient photocatalytic removal of rhodamine B. *J. Mater. Sci. Mater. Electron.*, *32*(17), 21880–21896. https://doi.org/10.1007/s10854-021-06532-y

[18] Dinari, M., Mohsen Momeni, M., Bozorgmehr, Z., & Karimi, S. (2016). Bismuth-containing layered double hydroxide as a novel efficient photocatalyst for degradation of methylene blue under visible light. J. Iran. Chem. Soc., *14, 695–701*. https://doi.org/10.1016/j.clay.2015.02.009

[19] Liu, Q., Ma, J., Wang, K., Feng, T., Peng, M., Yao, Z., et al. (2017). BiOCl and TiO_2 deposited on exfoliated ZnCr-LDH to enhance visible-light photocatalytic decolorization of Rhodamine B. *Ceram. Int.*, *43*(7), 5751–5758. https://doi.org/10.1016/j.ceramint.2017.01.119

[20] Huang, D., Ma, J., Yu, L., Wu, D., Wang, K., Yang, M., et al. (2015). AgCl and BiOCl composited with NiFe-LDH for enhanced photo-degradation of Rhodamine B. *Sep. Purif. Technol.*, *156*, 789–794. https://doi.org/10.1016/j.seppur.2015.11.003

[21] Fu, R., Gong, Y., Li, C., Niu, L., & Liu, X. (2021). CdIn2S4 / In (OH)3 / NiCr-LDH multi-interface heterostructure photocatalyst for enhanced photocatalytic H2 evolution and Cr(VI) reduction. *Nanomaterials*, *11*(11), 3122. https://doi.org/10.3390/nano11113122

[22] Sahoo, D. P., Nayak, S., Reddy, K. H., Martha, S., & Parida, K. (2018). Fabrication of a Co(OH)2/ZnCr-LDH "p-n" heterojunction photocatalyst with enhanced separation of charge carriers for efficient visible-light-driven H_2 and O_2 evolution. *Inorg. Chem.*, *57*(7), 3840–3854. https://doi.org/10.1021/acs.inorgchem.7b03213

[23] Baliarsingh, N., Parida, K. M., & Pradhan, G. C. (2014). Effects of Co, Ni, Cu, and Zn on photophysical and photocatalytic properties of carbonate intercalated MII/Cr LDHs for enhanced photodegradation of methyl orange. *Ind. Eng. Chem. Res.*, *53*(10), 3834–3841. https://doi.org/10.1021/ie403769b

[24] Li, H., Mao, C., Shang, H., Yang, Z., Ai, Z., & Zhang, L. (2018). New opportunities for efficient N2 fixation by nanosheet photocatalysts. *Nanoscale*, *10*(33), 15429–15435. https://doi.org/10.1039/c8nr04277b

[25] Nayak, S., & Parida, K. (2022). Superlative photoelectrochemical properties of 3D MgCr-LDH nanoparticles influencing towards photoinduced water splitting reactions. *Sci. Rep.*, *12*(1), 1–23. https://doi.org/10.1038/s41598-022-13457-x

[26] Sadeghi Rad, T., Sevval Yazici, E., Khataee, A., Gengec, E., & Kobya, M. (2023). Tuned CuCr layered double hydroxide/carbon-based nanocomposites inducing sonophotocatalytic degradation of dimethyl phthalate. *Ultrason. Sonochem.*, *95*, 106358. https://doi.org/10.1016/j.ultsonch.2023.106358

[27] Salehi, G., Bagherzadeh, M., Abazari, R., Hajilo, M., & Taherinia, D. (2024). Visible light-driven photocatalytic degradation of methylene blue dye using a highly efficient Mg-Al LDH@g-C_3N_4@Ag_3PO_4 nanocomposite. *ACS Omega*, *9*(4), 4581–4593. https://doi.org/10.1021/acsomega.3c07326

[28] Meng, L., Fu, G., Lan, Y., & Feng, L. (2014). Significantly enhanced visible-light-induced photocatalytic performance of hybrid Zn-Cr layered double hydroxide/graphene nanocomposite and the mechanism study. *Ind. Eng. Chem. Res.*, *53*(33), 12943–12952. https://doi.org/10.1021/ie501650g

[29] Ameur, N., Fandi, Z., Taieb-Brahimi, F., Ferouani, G., Bedrane, S., Bachir, R., et al. (2021). A novel approach of ceria nanotubes and plasmonic metal-doped ceria nanotubes application: Anticorrosion and photodegradation potential. *Appl. Phys. A*, *127*(3), 1–12. https://doi.org/10.1007/s00339-021-04292-4

[30] Erjeno, D. J. D., Asequia, D. M. A., Osorio, C. K. F., Omisol, C. J. M., Etom, A. E., Hisona, R. M. R., et al. (2024). Facile synthesis of band gap-tunable kappa-carrageenan-mediated C,S-doped TiO_2 nanoparticles for enhanced dye degradation. *ACS Omega*, *9*(19), 21245–21259. https://doi.org/10.1021/acsomega.4c01370

[31] Naceur, B., Abdelkader, E., Nadjia, L., Sellami, M., & Noureddine, B. (2016). Synthesis and characterization of Bi1.56Sb1.48Co0.96O7 pyrochlore sun-light-responsive photocatalyst. *Mater. Res. Bull.*, *74*, 491–501. https://doi.org/10.1016/j.materresbull.2015.11.012

[32] Nadjia, L., Abdelkader, E., Naceur, B., & Ahmed, B. (2018). CeO_2 nanoscale particles: Synthesis, characterization and photocatalytic activity under UVA light irradiation. *J. Rare Earths*, *36*(6), 575–587. https://doi.org/10.1016/j.jre.2018.01.004

[33] Sadeghi Rad, T., Sevval Yazici, E., Khataee, A., Gengec, E., & Kobya, M. (2023). Tuned CuCr layered double hydroxide/carbon-based nanocomposites inducing sonophotocatalytic degradation of dimethyl phthalate. *Ultrason. Sonochem.*, *95*, 106358. https://doi.org/10.1016/j.ultsonch.2023.106358

[34] Peng, W. C., Chen, Y. C., He, J. L., Ou, S. L., Horng, R. H., & Wuu, D. S. (2018). Tunability of p- and n-channel TiOx thin film transistors. *Sci. Rep.*, *8*(1), 1–11. https://doi.org/10.1038/s41598-018-27598-5

[35] Kang, S., Pawar, R. C., Pyo, Y., Khare, V., & Lee, C. S. (2016). Size-controlled BiOCl–RGO composites having enhanced photodegradative properties. *J. Exp. Nanosci.*, *11*(4), 259–275. https://doi.org/10.1080/17458080.2015.1047420

[36] Ali, B., Abdelkader, E., Naceur, B., Houcine, C., Nadjia, L., & Nourredine, B. (2023). Sunlight-driven photocatalytic degradation of Rhodamine B by BiOCl and TiO_2 deposited on NiCr-LDH. *Int. J. Environ. Anal. Chem.*, *103*(18), 6722–6741. https://doi.org/10.1080/03067319.2021.1959570

[37] Sahoo, D. P., Patnaik, S., & Parida, K. (2021). An amine functionalized ZnCr-LDH/MCM-41 nanocomposite as efficient visible light induced photocatalyst for Cr(VI) reduction. *Mater. Today Proc.*, *35*, 252–257. https://doi.org/10.1016/j.matpr.2020.05.526

[38] Oladipo, A. A. (2021). Rapid photocatalytic treatment of high-strength olive mill wastewater by sunlight and UV-induced $CuCr_2O_4$@CaFe–LDO. *J. Water Process Eng.*, *40*, 101932. https://doi.org/10.1016/j.jwpe.2021.101932

[39] Zhang, F., Zhang, C. L., Song, L., Zeng, R. C., Cui, L. Y., & Cui, H. Z. (2015). Corrosion resistance of superhydrophobic mg-al layered double hydroxide coatings on aluminum alloys. *Acta Metall. Sin. Engl. Lett.*, *28*(11), 1373–1381. https://doi.org/10.1007/s40195-015-0335-4

[40] Xie, W., Li, R., & Xu, Q. (2018). Enhanced photocatalytic activity of Se-doped TiO_2 under visible light irradiation. *Sci. Rep.*, *8*(1), 1–11. https://doi.org/10.1038/s41598-018-27135-4

[41] Zhang, J., Wang, Z., Fan, M., Tong, P., Sun, J., Dong, S., et al. (2019). Ultra-light and compressible 3D BiOCl/RGO aerogel with enriched synergistic effect of adsorption and photocatalytic degradation of oxytetracycline. *J. Mater. Res. Technol.*, *8*(5), 4577–4587. https://doi.org/10.1016/j.jmrt.2019.08.002

[42] Fathirad, F., Ziaadini, F., Mostafavi, A., & Shamspur, T. (2021). Three-layer magnetic nanocomposite containing semiconductor nanoparticles as catalyst for dye removal from water solutions under visible light. *Iran. J. Chem. Chem. Eng.*, *40*(6), 1749–1756.

[43] Ziaadini, F., Mostafavi, A., Shamspur, T., & Fathirad, F. (2019). Photocatalytic degradation of methylene blue from aqueous solution using Fe_3O_4@SiO_2@CeO_2 core-shell magnetic nanostructure as an effective catalyst. *Adv. Environ. Technol.*, *5*(2), 127–132. https://doi.org/10.22104/AET.2020.4137.1204

[44] Mangeli, A., Mostafavi, A., Shamspur, T., Fathirad, F., & Mehrabi, F. (2021). Decontamination of fenitrothion from aqueous solutions using rGO/MoS2/Fe_3O_4 magnetic nanosorbent: Synthesis, characterization and removal application. *J. Environ. Health Sci. Eng.*, *19*(2), 1505–1511. https://doi.org/10.1007/s40201-021-00706-w

How to cite this paper:

Bouteiba, A., Benhadria, N. & Bettahar, N. (2026). Highly efficient sunlight-powered photocatalytic degradation of rhodamine B Using Cu_2Cr-LDH/TiO_2 and Cu_2Cr-LDH/BiOCl semiconductor nanocomposites. Advances in Environmental Technology, 12(3), 291-307. DOI: 10.22104/aet.2026.7739.2177